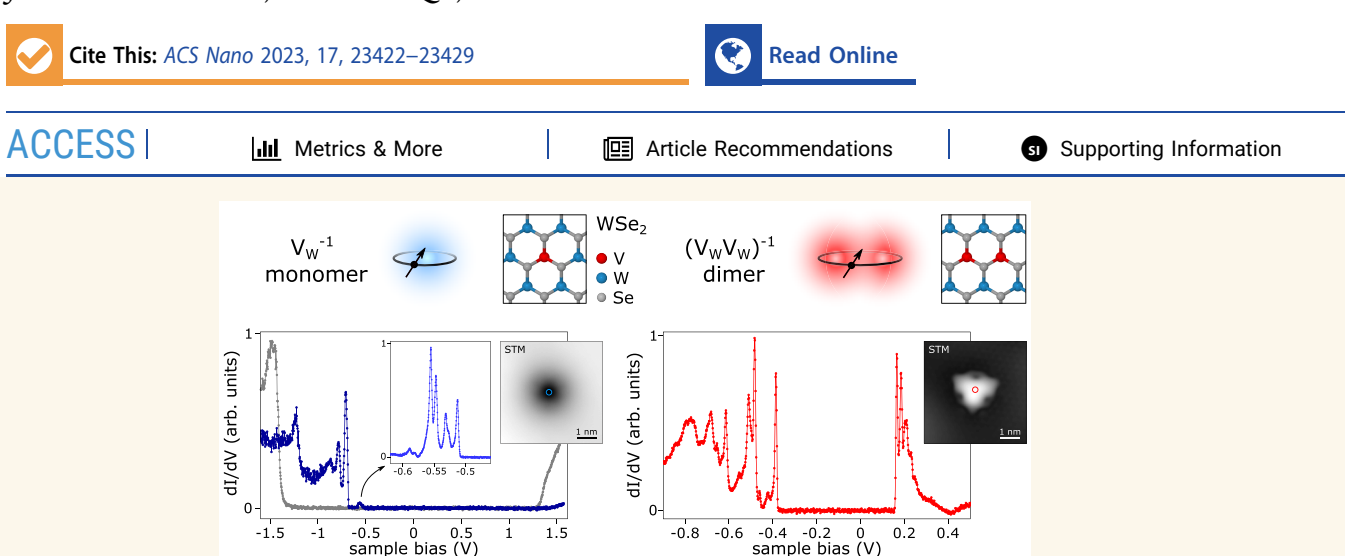


www.acsnano.org

Spin-Stabilization by Coulomb Blockade in a Vanadium Dimer in WSe₂

Samuel Stolz, Bowen Hou, Dan Wang, Azimkhan Kozhakhmetov, Chengye Dong, Oliver Gröning, Joshua A. Robinson, Diana Y. Qiu, and Bruno Schuler*



ABSTRACT: Charged dopants in 2D transition metal dichalcogenides (TMDs) have been associated with the formation of hydrogenic bound states, defect-bound trions, and gate-controlled magnetism. Charge-transfer at the TMD-substrate interface and the proximity to other charged defects can be used to regulate the occupation of the dopant's energy levels. In this study, we examine vanadium-doped WSe₂ monolayers on quasi-freestanding epitaxial graphene, by high-resolution scanning probe microscopy and ab initio calculations. Vanadium atoms substitute W atoms and adopt a negative charge state through charge donation from the graphene substrate. V_{W}^{-1} dopants exhibit a series of occupied p-type defect states, accompanied by an intriguing electronic fine-structure that we attribute to hydrogenic states bound to the charged impurity. We systematically studied the hybridization in V dimers with different separations. For large dimer separations, the 2e charge state prevails, and the magnetic moment is quenched. However, the Coulomb blockade in the nearest-neighbor dimer configuration stabilizes a 1e⁻ charge state. The nearest-neighbor V-dimer exhibits an open-shell character for the frontier defect orbital, giving rise to a paramagnetic ground state. Our findings provide microscopic insights into the charge stabilization and many-body effects of single dopants and dopant pairs in a TMD host material.

KEYWORDS: Point defects, 2D materials, Transition metal dichalcogenide, Scanning probe microscopy, Density functional theory

INTRODUCTION

Downloaded via PENNSYLVANIA STATE UNIV on March 25, 2024 at 14:33:22 (UTC). See https://pubs.acs.org/sharingguidelines for options on how to legitimately share published articles.

Chemical doping is the prime method for controlling the electronic and optical properties of bulk semiconductors. In two-dimensional (2D) semiconductors, this approach is less efficient because of the generally large defect ionization energies involved.1 While the hydrogen-like impurity model of dopant-bound electronic states has served very well for shallow dopants in bulk semiconductors, it fails to accurately describe the defect wave functions in 2D, which are sensitive to the extrinsic dielectric environment, 2,3 and prone to interfacial charge transfer.4 However, the inherent charge localization at dopants in 2D semiconductors offers exciting pathways to explore strong many-body physics and to control the magnetic

properties via the dopant's electron spin.5 Transition metal dichalcogenides (TMDs) are particularly suited for this purpose due to the established scalable synthesis of various types of substitutionally doped TMDs such as V, 6 Re, 7,8 Nb, 9 and Mn. 10 Despite the significant impact of point defects in

Received: May 30, 2023 Revised: October 25, 2023 Accepted: October 26, 2023 Published: November 17, 2023





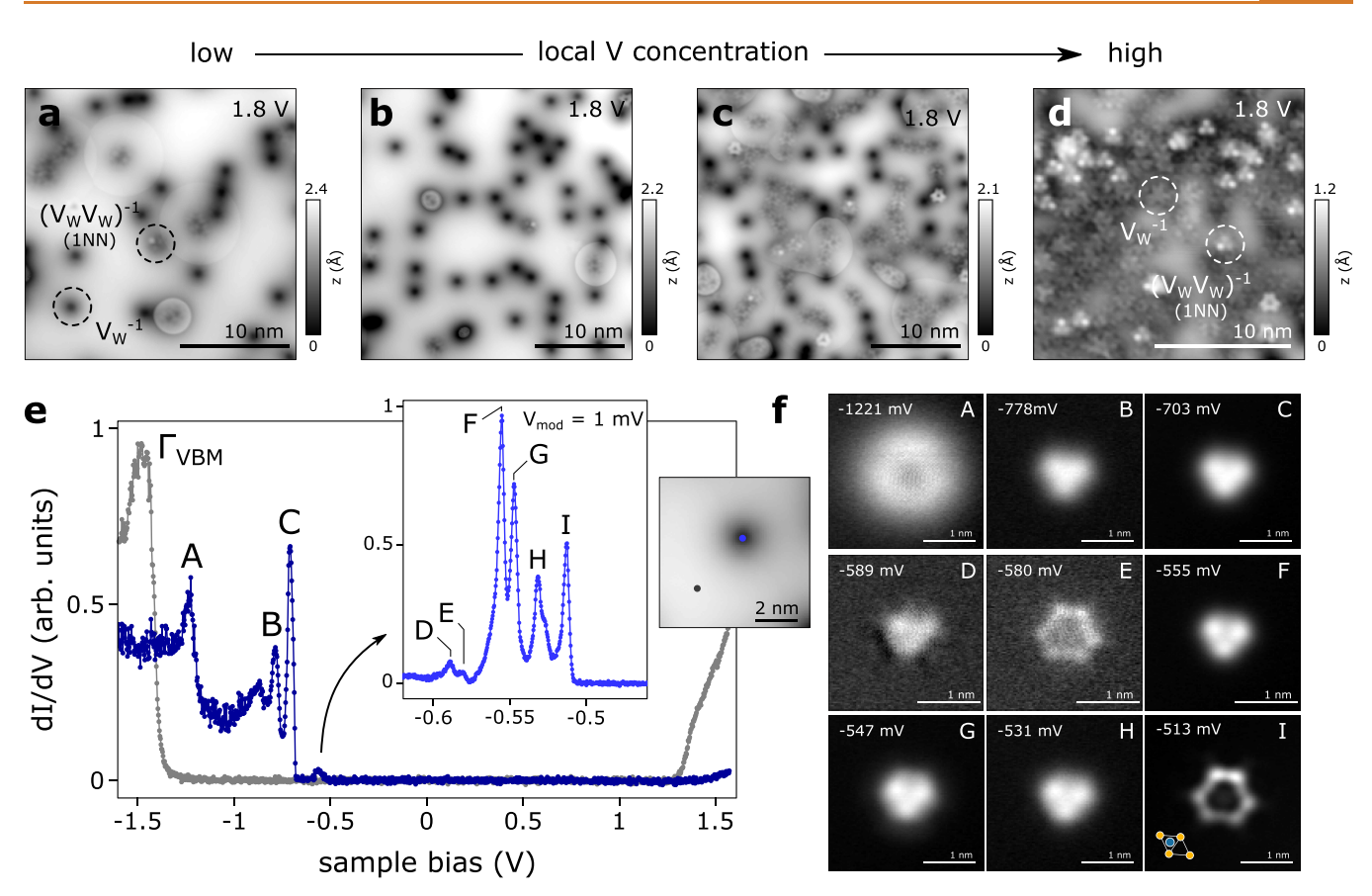


Figure 1. Single vanadium dopant in WSe₂. (a–d) STM topographies (I = 100 pA, V = 1.8 V) of V-doped (0.5%) monolayer WSe₂ on QFEG with substantial variations of the local V concentration. At low defect densities (a,b), single $V_{\rm w}^{-1}$ are imaged as dark depressions at positive bias due to their negative charge. At higher V concentrations (c,d), the V impurities adopt a flower-like contrast as the density of nearest-neighbor V dimers ($V_{\rm w}V_{\rm w}$)⁻¹ (1NN) increases. (e) dI/dV spectroscopy of an isolated $V_{\rm w}^{-1}$ in monolayer WSe₂ (dark blue: $V_{\rm mod} = 5$ mV. light blue: $V_{\rm mod} = 1$ mV). The main defect resonances are labeled. An intriguing fine structure (peaks D–I) at higher binding energies than the dominant defect resonance C is resolved when reducing the tip–sample separation. The inset STM topography indicates the spectroscopy location on the V dopant (blue circle) and substrate (gray circle). (f) Constant height dI/dV maps ($V_{\rm mod} = 2$ mV) at the sample voltages labeled in (e). The WSe₂ unit cell is displayed at the bottom left in panel I (blue: W, yellow: Se).

TMDs (intentional or otherwise), a comprehensive understanding of charge localization at TMD dopants and dopant—dopant interactions remains largely elusive at the microscopic level.

In this article, we use high-resolution scanning probe microscopy to study the effects of charge localization and dopant—dopant interactions between V substitutional dopants in WSe₂ on the atomic scale. Substitutional V-doping in WSe₂ has been shown to create a room temperature dilute semiconducting ferromagnet through the coupling of magnetic ions via itinerant spin-polarized charge carriers. ^{11–14} Critical in this regard is the charge state of the dopant, which can be controlled by adjusting the electrochemical potential of the host TMD through methods such as charge-transfer doping by the substrate⁴ and electrostatic gating. ¹⁵ Here we control the dopant charge state and electron spin by the proximity to other dopants and discover an intriguing electronic fine-structure associated with the charged impurities.

Specifically, we investigate the interaction between vanadium dopants in WSe_2 monolayers grown on quasi-free-standing graphene on 6H-SiC(0001) (QFEG/SiC) as a function of the separation distance between the dopants by means of scanning probe microscopy/spectrocopy (STM/STS), density functional theory (DFT), and *ab initio* many-

body perturbation theory. The V impurities adopt a negative charge state V_W⁻¹, even in the limit of high doping concentrations on the order of 1%. At such high V concentrations, spontaneous dimerization becomes more frequent, providing an opportunity to study the distancedependent interaction between V dopants. We find that, down to second-nearest-neighbor (2NN) V-V separation, both defects are singly charged and the dimer hosts 2 e-. However, the strong Coulomb interaction in the nearest-neighbor (1NN) dimer configuration results in an open-shell paramagnetic ground state with a nominal charge state of 1 e^- . For both, the isolated V_W^{-1} as well as for V dimers, we find a characteristic series of low-intensity resonances at higher binding energies than those of the main defect states in our STS data that we attribute to hydrogenic states bound to the charged impurity.

RESULTS AND DISCUSSION

V-Doped WSe₂ Monolayers with Varying V Concentrations. A V-doped monolayer WSe₂ was grown on quasifreestanding graphene on 6H-SiC(0001) (QFEG/SiC) using metal—organic chemical vapor deposition (MOCVD). Several samples were studied with a nominal V concentration of 0.5% (per W atom), as verified by X-ray photoelectron

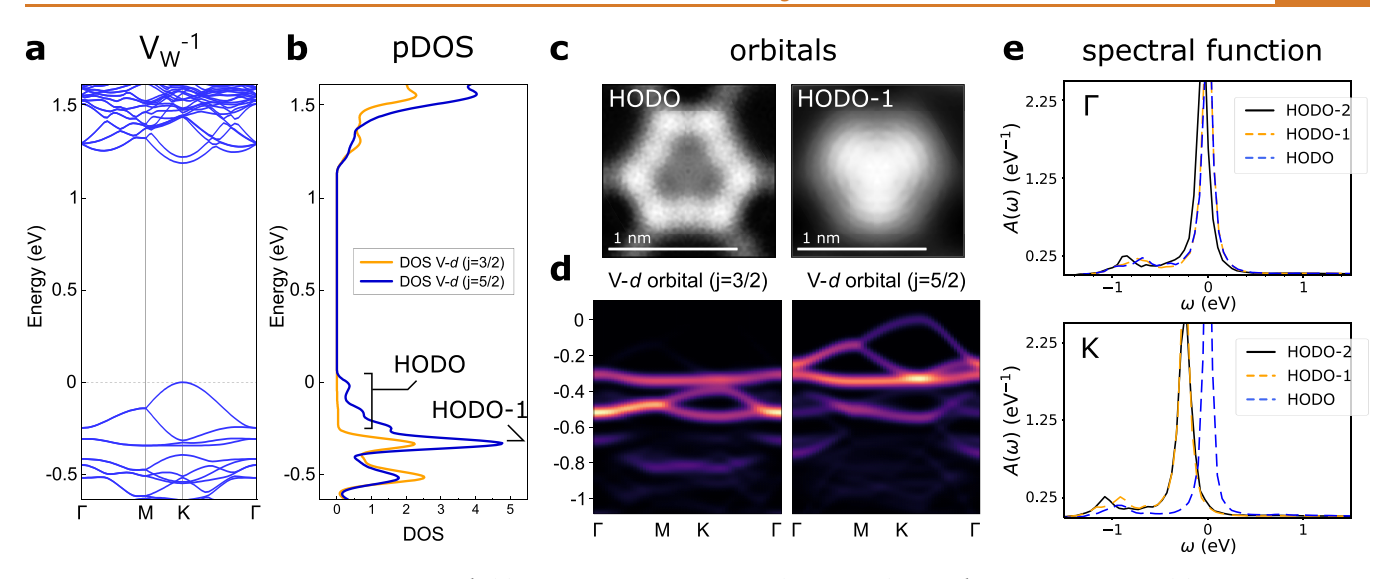


Figure 2. Calculated electronic structure of V_W^{-1} . (a) Calculated band structure (PBE+SOC) for V_W^{-1} in a 5 × 5 unit cell. (b) Projected density of states (pDOS) of V_W^{-1} onto the V d orbitals with a total angular momentum of j=3/2 and j=5/2. (c) Constant height map of the electron density of the HODO and HODO-1 state labeled in (b). (d) Projected band structure onto Vd orbitals. (e) Many-body spectral functions of V_W^{-1} at the Γ and K points. The elastic HODO peak has been chosen as a zero energy reference.

spectroscopy (XPS). Using STM, we observe substantial variations of the local V density ranging from 0.15% to 4% (see Figure S1) in several samples. These fluctuations can occur within a relatively abrupt transition region of a few nanometers. We take advantage of this naturally occurring inhomogeneity of the dopant distribution to study isolated single V impurities and V dimers of different spacing. In Figure 1a-d STM topographies of V-doped WSe₂ with different local V concentrations are shown. Close to the WSe₂ conduction band edge at a positive sample bias, isolated V dopants are imaged as dark featureless depressions. This is due to their negative charge and the associated upward band bending as reported previously. 6,18,19 At higher V concentrations, the appearance changes to a flower-like contrast. Moreover, V dimers (denoted as $(V_W V_W)^{-1}$ in Figure 1a,d) are more frequently observed. Independent of the separation between the V_W defects, V impurities substitute W in the WSe₂ lattice, as measured by CO-tip nc-AFM (Figure S4d).

Electronic Fine-Structure of Single V_W^{-1} in WSe₂ Monolayer. To set the basis for further investigations of V_W dimers, a rigorous characterization of single, isolated V impurities is needed. The dI/dV spectrum of a single, isolated V_W^{-1} impurity is presented in Figure 1e. We observe three dominant resonances (labeled A-C in Figure 1e) between the Γ valence band maximum (VBM) and the Fermi energy. These p-type V_W states are found only in the occupied spectrum and contrast with the observations in ref 14, which report in-gap defect states in both the occupied and unoccupied states, but are consistent with the results reported in ref 18. In addition to the three prominent $\mathrm{d}I/\mathrm{d}V$ peaks, we consistently observe a striking series of low-intensity dI/dV resonances (labeled D-I in Figure 1e) in the bias range of [-0.6 V, -0.5 V]. These resonances, which can only be resolved by increasing the energy resolution in our STS experiments, have a ten times lower intensity than the dominant defect peaks, with a full width at half-maximum (fwhm) as small as 3 meV, as determined from fits to Voigt functions (see Figure S7). The energy difference between the dominant dI/dV peak (C) and the low intensity peak (I) is 164 meV. Additional low-intensity

peaks (F–H) are found between C and I, with energy differences of 18.9 meV, 34.4 meV, and 42.6 meV with respect to I. While a broad low-intensity peak has been previously reported, ¹⁸ the intriguing fine-structure consisting of a series of peaks has not been resolved so far.

The spatial mapping of all localized defect resonances is shown in Figure 1f, and it reveals three distinct orbital shapes. The first shape is an extended donut-like orbital (A) resembling a *p*-like hydrogenic state, which has previously been reported for another negatively charged TMD defect. The second shape is a trilobal orbital (B–D and F–H) comprising the main defect resonance and is also repeated in some of the low-intensity STS peaks. Finally, a hexagonally shaped orbital (E,I) forms the highest occupied defect orbital.

To gain a better understanding of the experimentally observed defect states of V_W^{-1} , we conducted density functional theory (DFT) calculations. The calculated V_W^{-1} band structure using a Perdew-Burke-Ernzerhof (PBE)²⁴ functional and spin-orbit coupling (SOC) in a 5 × 5 WSe₂ unit cell is shown in Figure 2a. We find two prominent localized flat-band states near the Γ VBM and another state with 170 meV lower energy, in agreement with previous studies. 11,25 The top of the valence band near K is dispersive and has significant contributions from V d electrons, as shown in the projected density of states (pDOS) onto the V d orbitals with j = 5/2 and 3/2 in Figure 2b,d. The corresponding spatial distribution of the highest occupied defect orbital level (HODO) and HODO-1, depicted in Figure 2c, accurately reproduce the trilobal and hexagonal shapes observed in the experimental $\mathrm{d}I/\mathrm{d}V$ maps. However, while the DFT-level calculations can replicate the shapes of the experimental defect states, they cannot account for the series of low-intensity resonances at higher binding energies. To address this issue, we calculated the spectral function within the GW approximation^{26,27} to capture the strong many-body interactions commonly found in TMDs and other low-dimensional materials. Figure 2e shows the spectral function within G₀W₀ at the Γ and K points. In addition to the primary excitation peaks from the HODO and HODO-1, we find a series of

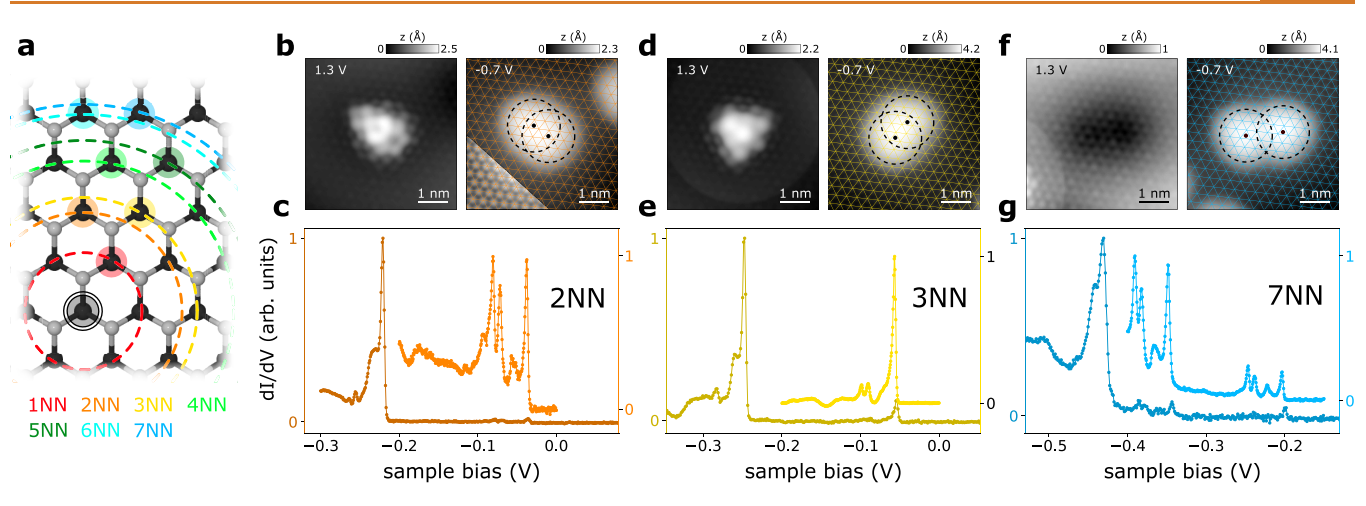


Figure 3. Evolution of dI/dV spectroscopy of vanadium dimers with different separations. (a) WSe₂ model (black: W, gray: Se) with different transition metal site pairs highlighted (1NN: nearest neighbor, 2NN: second nearest neighbor, etc.). (b) STM topography (I = 100 pA) of the 2NN dimer at 1.3 V and -0.7 V, respectively. In the bottom left corner of the right panel a different contrast was chosen to highlight the atomic contrast of the Se sublattice, which is indicated by the grid. The black dashed circles indicate the circumference of the circular STM contrast, with their center at the black dots assigning the lattice site of the V impurities. (c) dI/dV spectroscopy recorded at the center of the 2NN dimer (dark orange: $V_{\text{mod}} = 2 \text{ mV}$), light orange: $V_{\text{mod}} = 1 \text{ mV}$). The light orange spectrum was recorded at a smaller tip–sample separation and has been vertically offset for clarity. (d,f) Analog to (b), but for the 3NN and 7NN dimer configurations, respectively. (e,g) Analog to (c), but for the 3NN and 7NN dimer configurations, respectively.

satellite peaks at lower energies for all defect orbitals that result from strong electron—electron interactions of the charged defects. These satellite peaks are absent if a neutral V is considered. While these satellite peaks are sensitive to the super cell size, we calculate the spectral functions for a 5×5 and 7×7 super cell and then perform a linear extrapolation to infinite distance (Figure S13). The resulting spread between the main quasiparticle peak and the closest satellite feature is 0.2 eV.

Our findings suggest that the series of low-intensity peaks resolved in high-resolution STS of V_W⁻¹ are a result of occupation of defect-bound states at the charged impurity.²⁰ While the relative energies of the fine-structure peaks overlap with the phononic density of states of monolayer WSe₂, ²⁸ they are unlikely to be of vibronic origin because inelastic excitations by tunneling electrons would be expected at energies higher than the elastic excitation peaks (more negative bias) and, therefore, cannot account for the low-intensity finestructure peaks. The ground state binding energy of the hydrogen-like series of a single V dopant in WSe2, 164 meV, is several times higher than that in bulk materials, ²⁹ analogous to the difference in exciton binding energies. ³⁰ Interestingly, binding energies similar to those of the observed low-intensity peaks have been reported in recent photoluminescence measurements of unidentified defects in WSe₂.³¹ It is worth noting that the vanadium dopants are negatively charged and that holes are injected into the sample at negative sample bias, rendering the creation of defect bound excitons and trions as a plausible mechanism as well. Further investigations are needed to explain the characteristic fine-structure motif and its potential link to similar optical signatures observed in other TMD samples.

Electronic Fingerprints of Vanadium Dimers. The electronic spectrum of V dopants can be influenced significantly by their proximity to other dopants due to their negative charge. We thus investigated the interaction between vanadium pairs as a function of their separation and found that their interaction evolves from purely electrostatic for large

separations to the formation of hybrid dimer orbitals at very close distances. In Figure 3, we present three types of dimers with different distances separating the two vanadium dopants. The nomenclature of *n* NN is used to refer to the *n*th nearest neighbor (NN) dimers, as sketched in Figure 3a. The STM topography at 1.3 V is characteristic for each dimer, as seen in Figure 3b,d,f. By resolving the Se sublattice (colored grid in Figure 3b,d,f) at -0.7 V, we can determine the exact lattice registry of the V dopants and thereby their dimer configuration. We studied 1NN, 2NN-5NN, 7NN, and 10NN dimers (see also Figure S6) and found that except for the 1NN dimer, all dimers exhibit similar STS features to those of the single V_W^{-1} : a prominent STS resonance in the range of [-0.5 V, -0.2 V] (Figure 3c,e,g darker shade) followed by a series of low-intensity peaks (Figure 3c,e,g lighter shade). Intriguingly, we observe two recurring fine-structure motifs: a series with five resonances similar to the single V_W^{-1} (found in the 2NN, 7NN and 10NN dimers, cf. Figure S7) and a series with three resonances (found in the 3NN-5NN dimer, cf. Figure S8). It is unclear why these patterns repeat, as there is no apparent systematic relationship to the dimer spacing or crystal direction.

Furthermore, we observe that the low-intensity peaks in the $\mathrm{d}I/\mathrm{d}V$ spectra replicate within the same spectrum, which is most evident for large dimer separations such as the 7NN dimer shown in Figure 3g. As the dimer separation decreases, the splitting between these duplicates increases, from 113 meV for the 10NN dimer to 183 meV for the 4NN dimer. For dimer separations less than 4NN, the higher energy branch of the fine-structure series merges with the dominant $\mathrm{d}I/\mathrm{d}V$ peak, making it difficult to distinguish between them. The bonding—antibonding-like splitting of the fine-structure series in V dimers can be explained as interactions between atom-like orbitals associated with the V dopants, where the interaction strength decreases with increasing V dopant separation.

Coulomb Blockade in Nearest Neighbor Vanadium Dimers. The nearest neighbor (1NN) dimer stands out among all of the dimers we studied. As seen in Figure 4, its dI/

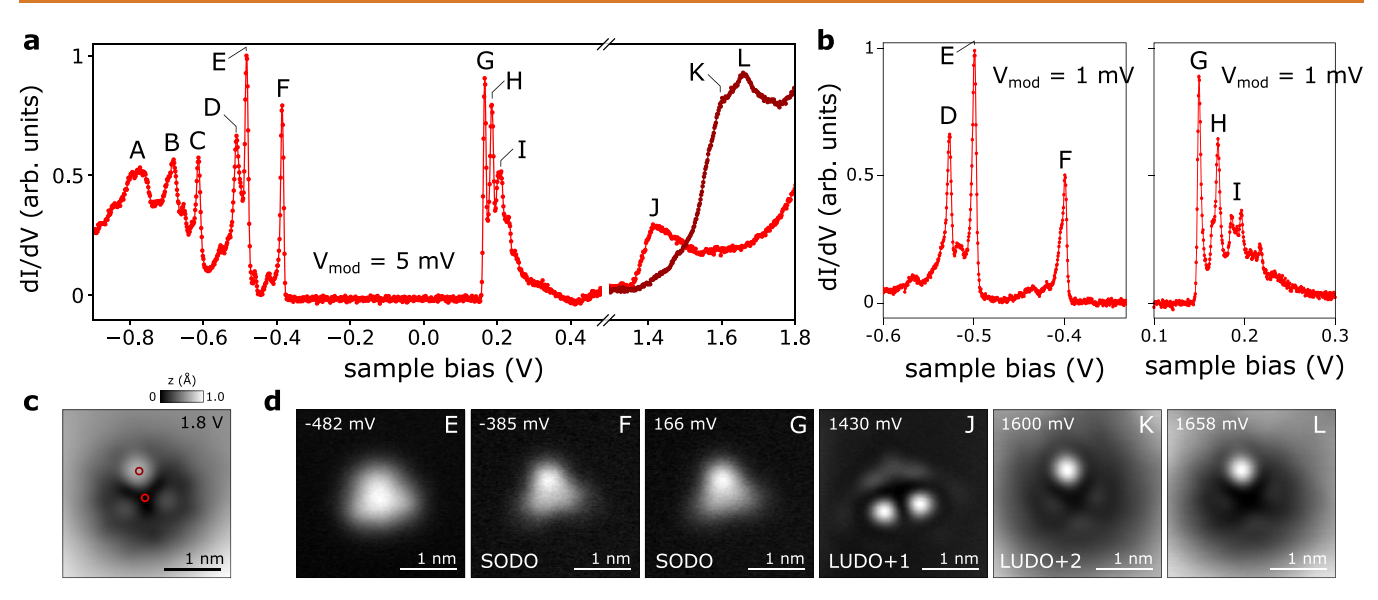


Figure 4. In-gap defect states of the nearest-neighbor (1NN) V dimer $(V_W V_W)^{-1}$. (a) dI/dV spectroscopy $(V_{mod} = 5 \text{ mV})$ of the 1NN dimer at the positions indicated in (c). The main defect states have been labeled. (b) High-resolution dI/dV spectroscopy $(V_{mod} = 1 \text{ mV})$ of the 1NN dimer states D–I. (c) STM topography (I = 100 pA) of the 1NN V dimer. (d) Constant height dI/dV maps $(V_{mod} = 2 \text{ mV})$ of selected resonances labeled in (a,b). The resemblance of the highest occupied (F) and lowest unoccupied defect orbitals (G) is indicative of a singly occupied defect state.

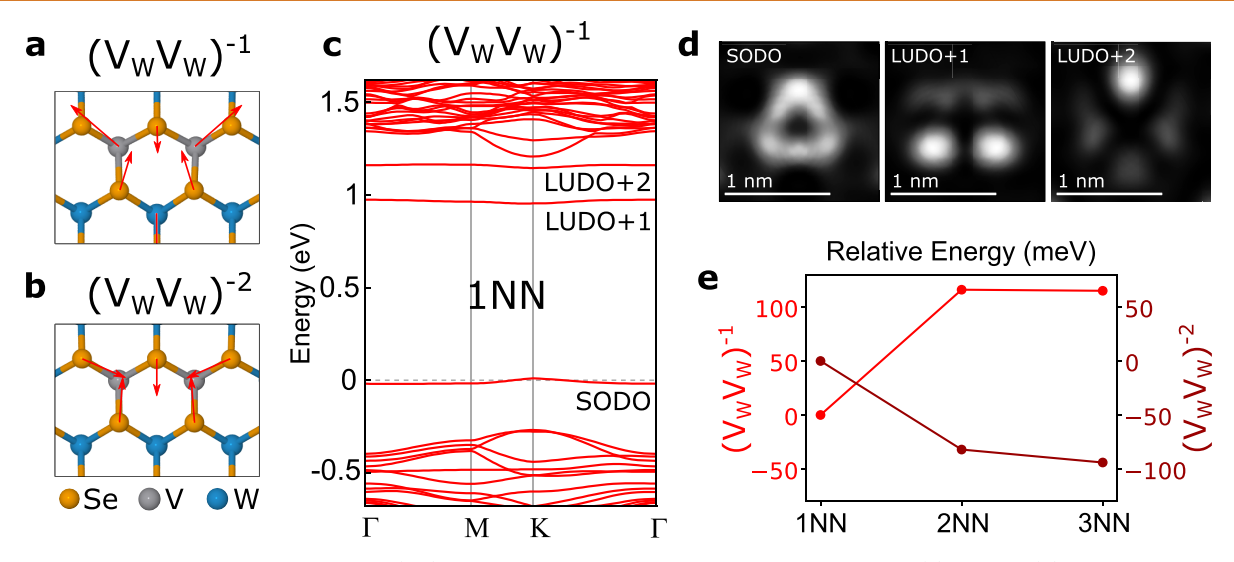


Figure 5. Vanadium dimers' DFT calculations. (a,b) Relaxed geometry of the 1NN V dimer in the $1e^-$ (a) and $2e^-$ (b) charge states exhibiting different local distortions of the WSe₂ lattice. The red arrows indicate the direction and magnitude of the relaxation compared to pristine WSe₂ for atoms that relax more than 5 pm. For clarity, the arrows are 50 times longer than the actual relaxation. (c) Calculated band structure of the 1NN dimer $(V_WV_W)^{-1}$ with PBE+DFT. (d) Constant height map of the electron densities of the V dimer states labeled in (c) that are in excellent agreement with the experimental dI/dV maps in Figure 4d. (e) Total energy of the V dimer in the 1NN-3NN configurations for the $1e^-$ (red) and $2e^-$ (dark red) charge states, relative to the 1NN energy.

dV signature of the occupied states is qualitatively different from those of all other dimers, as there is no observation of any low-intensity fine-structure in the 1NN dimer. Moreover, 1NN is the only dimer that also features multiple defect states in the unoccupied spectrum (G–L). The defect orbital G and its satellite peaks H,I resemble a characteristic Franck–Condonlike vibronic progression with a dominant mode at 21 meV, similar to previous findings on S vacancies³² and C substituted S defects in WS₂.³³

The resonances at negative bias are less likely to originate from vibronic excitations, as their energy differences are larger and no characteristic sequence is observed. Mapping of the 1NN V dimer defect orbitals (see Figure 4d and Figure S9d)

indicates that the defect has an open-shell character with a similar shape of the highest occupied (F) and lowest unoccupied (G) defect orbitals. Therefore, we assign the resonances F and G to the same singly occupied defect orbital (SODO). The different level occupations of the nearest neighbor V dimer are attributed to a different charge state. The V dimer in the 1NN configuration can only accommodate a $1e^-$ charge state $(V_WV_W)^{-1}$, whereas for all other dimers, a doubly negative charge state is adopted $(V_WV_W)^{-2}$. The openshell character in the 1NN dimer therefore arises from the Coulomb blockade, driven by the stronger confinement of the 1NN dimer states.

Our calculations confirm that the 1NN dimer favors the 1e⁻ charge state, whereas the 2e- charge state becomes energetically more favorable with larger V-V separations. The relaxed geometries of the 1NN $(V_W V_W)^{-1}$ and the 1NN $(V_W V_W)^{-2}$ defects are depicted in Figure 5a,b, showing an outward relaxation of the two neighboring V atoms at 1e- charge and no change in the position of the V dimers at 2e⁻ charge. In our band structure calculations of the 1NN $(V_W V_W)^{-1}$ dimer (Figure 5c), we observe three in-gap defect states, a singly occupied defect orbital (SODO) and two unoccupied orbitals (LUDO+1, LUDO+2). The calculated electron densities of the defect states shown in Figure 5d are in excellent agreement with the experimental dI/dV maps in Figure 4d. The calculated total energies for different V dimer configurations shown in Figure 5e reveal that the 1e⁻ charge state is most favorable for the 1NN dimer, while at larger V separations $2e^-$ is preferred. Even though a direct comparison between the total energies of different charge states is not possible, the calculated trends are in agreement with the experimental observations. Consequently, we find that the odd number of electrons in the 1NN dimer $(V_W V_W)^{-1}$ yields a magnetic moment of 1 μB , which is quenched for all other dimer configurations. Thus, the stabilization of the 1e⁻ charge state in the 1NN V dimer results in a paramagnetic defect configuration.

CONCLUSIONS

Our study provides a comprehensive analysis of charged individual V dopants and dopant pairs in WSe_2 , expanding our understanding of the electronic properties of doped transition metal dichalcogenides. We observed a previously unknown spectroscopic fine-structure resulting from many-body effects arising from the negative charge localized at the defect, which was present not only in the V_W^{-1} monomer but also in various V dimers with two repeating motifs. Our analysis of the interaction between charged V atoms showed that the nearest neighbor dimer can accommodate only a single charge $(V_W V_W)^{-1}$, while dimers with greater separations are doubly charged $(V_W V_W)^{-2}$. As a result, the 1NN dimer exhibits an open-shell paramagnetic ground state, while the magnetic moment is quenched for the V_W⁻¹ monomer and other (V_WV_W)⁻² dimer configurations. These findings establish proximity-controlled charge state stabilization as a promising approach to regulate the magnetic properties.

METHODS

MOCVD Growth of V-Doped WSe₂ Monolayers. The V-doped WSe₂ samples were synthesized in a custom-designed vertical cold wall gas-source CVD reactor as reported previously in refs 16,34. Tungsten hexacarbonyl (W(CO)₆) (99.99%, Sigma-Aldrich), hydrogen selenide (H₂Se) (99.99%, Matheson), and vanadium (V(C₅H₅)₂) (sublimed, 95% Strem Chemicals) were used as metal, chalcogen, and dopant precursors, respectively, in a 100% H₂ ambient.

The metal and dopant precursors were kept inside stainless-steel bubblers where temperature and pressure were constantly maintained at 25 °C and 970 mbar and 40 °C and 970 mbar, respectively. $\rm H_2Se$ was supplied from a separate gas manifold. All three precursors were introduced from separate lines to prevent intermixing before reaching the reactor inlet. The growth of V-doped WSe₂ followed the three-step growth reported in ref 35, which consists of a nucleation, a ripening, and a lateral growth stage on c-plane sapphire (Cryscore Optoelectronic LTd, 99.95%.). At all three stages, the growth temperature, pressure, and $\rm H_2Se$ flow rate were kept constant at 800 °C, 930 mbar, and 7 sccm.

For the nucleation phase, the metal and dopant precursors were inserted with a flow rate of 20 and 60 sccm, respectively, for 2 min. At the ripening stage, the metal and dopant precursor flows were switched off and the formed nuclei were annealed in $\rm H_2Se$ for 10 min. During the lateral growth phase, $\rm W(CO)_6$ and $\rm V(C_3H_5)_2$ were reintroduced with a constant flow of 4.5 and 5 sccm, respectively. The vanadium density was deduced from STM measurements.

Scanning Probe Measurements. V-doped WSe₂ was prepared ex situ on QFEG on SiC substrates followed by a final 450 °C anneal in ultrahigh vacuum. The measurements were performed with a commercial LT STM from Scienta Omicron operated at 5 K and at pressures below 2×10^{-10} mbar. The tungsten tip was prepared on a clean Au(111) surface (sputtering: 10 min, Ar⁺, 1 kV; annealing: 10 min, 450 °C) and confirmed to be metallic. For nc-AFM experiments, the metallic tip was modified with a single CO molecule³⁶ that was picked up from the Au(111) surface. STM topographic measurements were taken in constant current mode with the bias voltage given with respect to the sample. STS measurements were recorded in constant height mode by using a lock-in amplifier at 860 Hz. The nc-AFM topographies were acquired in constant height mode with the Qplus sensor driven at its resonance frequency of ≈25 kHz with a constant amplitude of 70 pm. The frequency shift from the resonance of the tuning fork was recorded using Omicron Matrix electronics and HF₂Li PLL from Zurich Instruments.

Density-Functional Theory (DFT) and GW Calculations. DFT calculations were performed with the Quantum ESPRESSO software package. ²³ Optimized norm-conserving Vanderbilt (ONCV) pseudopotentials ³⁷ with the Perdew–Burke–Ernzerhof (PBE) functional ²⁴ were used to optimize the geometric structure and to obtain the electronic structure at the DFT level. A cutoff energy of 85 Ry was used for the plane-wave basis, and the convergence condition for the total energy change in two consecutive self-consistent calculation steps was less than 10^{-10} Ry. Defect calculations were performed in a $5 \times 5 \times 1$ WSe₂ supercell, and the k-space was sampled with a $3 \times 3 \times 1$ k-grid. Spin—orbit coupling was included through a relativistic spinor formalism.

The spectral function of V_W^{-1} was investigated by the BerkeleyGW package calculated within a one-shot full-frequency GW approach $^{38-40}$ as implemented in the BerkeleyGW software package. 27 Calculations were performed for defects in 5 \times 5 \times 1 and 7 \times 7 \times 1 supercells. A cutoff of 15 Ry was used for plane-components of the dielectric matrix, and 1000 bands were included in the sum over bands in the calculation of the polarizability and self-energy. A 3 \times 3 \times 1 k-point sampling was used with an additional subsampling of 10 k-points in the Voronoi cell. 41

ASSOCIATED CONTENT

Supporting Information

The Supporting Information is available free of charge at https://pubs.acs.org/doi/10.1021/acsnano.3c04841.

STM images on V densities/distributions; Bias dependent contrast and charging rings; Atomically resolved CO-tip nc-AFM measurements and simulations; dI/dV spectroscopy of V dimers at different separations and peak fitting of their electronic fine-structure; dI/dV maps of 1NN V dimer orbitals; Along the line dI/dV spectra across different V configurations; Bader charge analysis of V monomer and dimers; Cell size extrapolation for spectral function convergence (PDF)

AUTHOR INFORMATION

Corresponding Author

Bruno Schuler — nanotech@surfaces Laboratory, Empa — Swiss Federal Laboratories for Materials Science and Technology, 8600 Dübendorf, Switzerland; ⊚ orcid.org/0000-0002-9641-0340; Email: bruno.schuler@empa.ch

Authors

- Samuel Stolz nanotech@surfaces Laboratory, Empa Swiss Federal Laboratories for Materials Science and Technology, 8600 Dübendorf, Switzerland; Department of Physics, University of California, Berkeley, California 94720, United States
- Bowen Hou Department of Mechanical Engineering and Materials Science, Yale University, New Haven, Connecticut 06511, United States
- Dan Wang Department of Mechanical Engineering and Materials Science, Yale University, New Haven, Connecticut 06511, United States
- Azimkhan Kozhakhmetov Department of Materials Science and Engineering, The Pennsylvania State University, University Park, Pennsylvania 16082, United States; Two-Dimensional Crystal Consortium, The Pennsylvania State University, University Park, Pennsylvania 16802, United States
- Chengye Dong Two-Dimensional Crystal Consortium, The Pennsylvania State University, University Park, Pennsylvania 16802, United States
- Oliver Gröning nanotech@surfaces Laboratory, Empa Swiss Federal Laboratories for Materials Science and Technology, 8600 Dübendorf, Switzerland
- Joshua A. Robinson Department of Materials Science and Engineering, The Pennsylvania State University, University Park, Pennsylvania 16082, United States; Two-Dimensional Crystal Consortium, The Pennsylvania State University, University Park, Pennsylvania 16802, United States; Department of Chemistry and Department of Physics, The Pennsylvania State University, University Park, Pennsylvania 16802, United States
- Diana Y. Qiu Department of Mechanical Engineering and Materials Science, Yale University, New Haven, Connecticut 06511, United States; orcid.org/0000-0003-3067-6987

Complete contact information is available at: https://pubs.acs.org/10.1021/acsnano.3c04841

Notes

The authors declare no competing financial interest.

ACKNOWLEDGMENTS

We thank Michael E. Flatté for helpful discussions. S.S. acknowledges funding from the Swiss National Science Foundation under project numbers 159690 and 195133. A.K., C.D., and J.A.R. acknowledge Intel through the Semiconductor Research Corporation (SRC) Task 2746 and the Penn State 2D Crystal Consortium Materials Innovation Platform (2DCC-MIP) under NSF cooperative agreement DMR-1539916 for financial support. Theory work by B.H., D.W., and D.Y.Q. was supported by the U.S. Department of Energy, Office of Science, Basic Energy Sciences, under Early Career Award No. DE-SC0021965. Development of the BerkeleyGW code was supported by the Center for Computational Study of Excited-State Phenomena in Energy Materials (C2SEPEM) at the Lawrence Berkeley National Laboratory, funded by the U.S. Department of Energy, Office of Science, Basic Energy Sciences, Materials Sciences and Engineering Division, under Contract No. DE-AC02-05CH11231. The calculations used resources of the National Energy Research Scientific Computing (NERSC), a DOE Office of Science User Facility operated under contract no. DE-AC02-05CH11231;

the Texas Advanced Computing Center (TACC) at The University of Texas at Austin; and the INCITE program at the Oak Ridge Leadership Computing Facility, which is a DOE Office of Science User Facility supported under Contract DE-AC05-00OR22725. B.S. appreciates funding from the European Research Council (ERC) under the European Union's Horizon 2020 research and innovation program (Grant agreement No. 948243).

REFERENCES

- (1) Zhu, G.-J.; Xu, Y.-G.; Gong, X.-G.; Yang, J.-H.; Yakobson, B. I. Dimensionality-Inhibited Chemical Doping in Two-Dimensional Semiconductors: The Phosphorene and MoS2 from Charge-Correction Method. *Nano Lett.* **2021**, *21*, 6711–6717.
- (2) Ugeda, M. M.; Bradley, A. J.; Shi, S.-F.; da Jornada, F. H.; Zhang, Y.; Qiu, D. Y.; Ruan, W.; Mo, S.-K.; Hussain, Z.; Shen, Z.-X.; et al. Giant bandgap renormalization and excitonic effects in a monolayer transition metal dichalcogenide semiconductor. *Nat. Mater.* **2014**, *13*, 1091
- (3) Raja, A.; Chaves, A.; Yu, J.; Arefe, G.; Hill, H. M.; Rigosi, A. F.; Berkelbach, T. C.; Nagler, P.; Schüller, C.; Korn, T.; Nuckolls, C.; Hone, J.; Brus, L. E.; Heinz, T. F.; Reichman, D. R.; Chernikov, A. Coulomb Engineering of the Bandgap and Excitons in Two-Dimensional Materials. *Nat. Commun.* **2017**, *8*, 15251.
- (4) Froehlicher, G.; Lorchat, E.; Berciaud, S. Charge Versus Energy Transfer in Atomically Thin Graphene-Transition Metal Dichalcogenide van der Waals Heterostructures. *Phys. Rev. X* **2018**, *8*, 011007.
- (5) Robinson, J. A.; Schuler, B. Engineering and probing atomic quantum defects in 2D semiconductors: A perspective. *Appl. Phys. Lett.* **2021**, *119*, 140501.
- (6) Kozhakhmetov, A.; Stolz, S.; Tan, A. M. Z.; Pendurthi, R.; Bachu, S.; Turker, F.; Alem, N.; Kachian, J.; Das, S.; Hennig, R. G.; Gröning, O.; Schuler, B.; Robinson, J. A. Controllable p-Type Doping of 2D WSe2 via Vanadium Substitution. *Adv. Funct. Mater.* **2021**, *31*, 2105252.
- (7) Zhang, K.; Bersch, B. M.; Joshi, J.; Addou, R.; Cormier, C. R.; Zhang, C.; Xu, K.; Briggs, N. C.; Wang, K.; Subramanian, S.; et al. Tuning the electronic and photonic properties of monolayer MoS2 via in situ rhenium substitutional doping. *Adv. Funct. Mater.* **2018**, 28, 1706950.
- (8) Kozhakhmetov, A.; Schuler, B.; Tan, A. M. Z.; Cochrane, K. A.; Nasr, J. R.; El-Sherif, H.; Bansal, A.; Vera, A.; Bojan, V.; Redwing, J. M.; et al. Scalable Substitutional Re-Doping and its Impact on the Optical and Electronic Properties of Tungsten Diselenide. *Adv. Mater.* **2020**, 32, 2005159.
- (9) Zhang, K.; Deng, D. D.; Zheng, B.; Wang, Y.; Perkins, F. K.; Briggs, N. C.; Crespi, V. H.; Robinson, J. A. Tuning transport and chemical sensitivity via niobium doping of synthetic MoS2. *Adv. Mater. Interfaces* **2020**, *7*, 2000856.
- (10) Zhang, K.; Feng, S.; Wang, J.; Azcatl, A.; Lu, N.; Addou, R.; Wang, N.; Zhou, C.; Lerach, J.; Bojan, V.; et al. Manganese doping of monolayer MoS2: the substrate is critical. *Nano Lett.* **2015**, *15*, 6586–6591.
- (11) Zhang, F.; Zheng, B.; Sebastian, A.; Olson, D. H.; Liu, M.; Fujisawa, K.; Pham, Y. T. H.; Jimenez, V. O.; Kalappattil, V.; Miao, L.; Zhang, T.; Pendurthi, R.; Lei, Y.; Elías, A. L.; Wang, Y.; Alem, N.; Hopkins, P. E.; Das, S.; Crespi, V. H.; Phan, M.-H.; et al. Monolayer Vanadium-Doped Tungsten Disulfide: A Room-Temperature Dilute Magnetic Semiconductor. *Adv. Sci.* **2020**, *7*, 2001174.
- (12) Yun, S. J.; Duong, D. L.; Ha, D. M.; Singh, K.; Phan, T. L.; Choi, W.; Kim, Y.-M.; Lee, Y. H. Ferromagnetic Order at Room Temperature in Monolayer WSe2 Semiconductor via Vanadium Dopant. *Adv. Sci.* **2020**, *7*, 1903076.
- (13) Pham, Y. T. H.; Liu, M.; Jimenez, V. O.; Yu, Z.; Kalappattil, V.; Zhang, F.; Wang, K.; Williams, T.; Terrones, M.; Phan, M.-H. Tunable Ferromagnetism and Thermally Induced Spin Flip in Vanadium-Doped Tungsten Diselenide Monolayers at Room Temperature. *Adv. Mater.* **2020**, *32*, 2003607.

- (14) Song, B.; Yun, S. J.; Jiang, J.; Avila, J.; Beach, K.; Choi, W.; Kim, Y.-M.; Yoon, D.; Terrones, H.; Song, Y. J.; Asensio, M. C.; Duong, D. L.; Lee, Y. H. Evidence of itinerant holes for long-range magnetic order in the tungsten diselenide semiconductor with vanadium dopants. *Phys. Rev. B* **2021**, *103*, 094432.
- (15) Radisavljevic, B.; Radenovic, A.; Brivio, J.; Giacometti, V.; Kis, A. Single-layer MoS2 transistors. *Nat. Nanotechnol.* **2011**, *6*, 147–150. (16) Kozhakhmetov, A.; Nasr, J. R.; Zhang, F.; Xu, K.; Briggs, N. C.; Addou, R.; Wallace, R.; Fullerton-Shirey, S. K.; Terrones, M.; Das, S.; Robinson, J. A. Scalable BEOL compatible 2D tungsten diselenide. *2D Mater.* **2020**, *7*, 015029.
- (17) Wang, S.; Ding, D.; Li, P.; Sui, Y.; Liu, G.; Zhao, S.; Xiao, R.; Tian, C.; Chen, Z.; Wang, H.; et al. Concentration Phase Separation of Substitution-Doped Atoms in TMDCs Monolayer. *Small* **2023**, *19*, 2301027.
- (18) Mallet, P.; Chiapello, F.; Okuno, H.; Boukari, H.; Jamet, M.; Veuillen, J.-Y. Bound Hole States Associated to Individual Vanadium Atoms Incorporated into Monolayer WSe2. *Phys. Rev. Lett.* **2020**, *125*, 036802.
- (19) Stolz, S.; Kozhakhmetov, A.; Dong, C.; Gröning, O.; Robinson, J. A.; Schuler, B. Layer-dependent Schottky contact at van der Waals interfaces: V-doped WSe2 on graphene. *npj 2D Mater. Appl.* **2022**, 666
- (20) Aghajanian, M.; Schuler, B.; Cochrane, K. A.; Lee, J.-H.; Kastl, C.; Neaton, J. B.; Weber-Bargioni, A.; Mostofi, A. A.; Lischner, J. Resonant and bound states of charged defects in two-dimensional semiconductors. *Phys. Rev. B* **2020**, *101*, 081201. (R)
- (21) Hohenberg, P.; Kohn, W. Inhomogeneous Electron Gas. *Phys. Rev.* **1964**, *136*, B864–B871.
- (22) Kohn, W.; Sham, L. J. Self-Consistent Equations Including Exchange and Correlation Effects. *Phys. Rev.* **1965**, *140*, A1133–A1138.
- (23) Giannozzi, P.; Baroni, S.; Bonini, N.; Calandra, M.; Car, R.; Cavazzoni, C.; Ceresoli, D.; Chiarotti, G. L.; Cococcioni, M.; Dabo, I.; Dal Corso, A.; de Gironcoli, S.; Fabris, S.; Fratesi, G.; Gebauer, R.; Gerstmann, U.; Gougoussis, C.; Kokalj, A.; Lazzeri, M.; Martin-Samos, L.; et al. QUANTUM ESPRESSO: a modular and open-source software project for quantum simulations of materials. *J. Phys.: Condens. Matt.* **2009**, *21*, 395502.
- (24) Perdew, J. P.; Burke, K.; Ernzerhof, M. Generalized gradient approximation made simple. *Phys. Rev. Lett.* **1996**, *77*, 3865.
- (25) Duong, D. L.; Kim, S.-G.; Lee, Y. H. Gate modulation of the long-range magnetic order in a vanadium-doped WSe2 semi-conductor. *AIP Adv.* **2020**, *10*, 065220.
- (26) Hybertsen, M. S.; Louie, S. G. Electron correlation in semiconductors and insulators: Band gaps and quasiparticle energies. *Phys. Rev. B* **1986**, *34*, 5390–5413.
- (27) Deslippe, J.; Samsonidze, G.; Strubbe, D.; Jain, M.; Cohen, M. L.; Louie, S. G. BerkeleyGW: A massively parallel computer package for the calculation of the quasiparticle and optical properties of materials and nanostructures. *Comput. Phys. Commun.* **2012**, *183*, 1269.
- (28) Fiore, S.; Luisier, M. Ab initio modeling of thermal transport through van der Waals materials. *Phys. Rev. Mater.* **2020**, *4*, 094005.
- (29) Jagannath, C.; Grabowski, Z.; Ramdas, A. Linewidths of the electronic excitation spectra of donors in silicon. *Phys. Rev. B* **1981**, 23, 2082.
- (30) Chernikov, A.; Berkelbach, T. C.; Hill, H. M.; Rigosi, A.; Li, Y.; Aslan, B.; Reichman, D. R.; Hybertsen, M. S.; Heinz, T. F. Exciton binding energy and nonhydrogenic Rydberg series in monolayer WS 2. *Phys. Rev. Lett.* **2014**, *113*, 076802.
- (31) Rivera, P.; He, M.; Kim, B.; Liu, S.; Rubio-Verdú, C.; Moon, H.; Mennel, L.; Rhodes, D. A.; Yu, H.; Taniguchi, T.; Watanabe, K.; Yan, J.; Mandrus, D. G.; Dery, H.; Pasupathy, A.; Englund, D.; Hone, J.; Yao, W.; Xu, X. Intrinsic donor-bound excitons in ultraclean monolayer semiconductors. *Nat. Commun.* **2021**, *12*, 871.
- (32) Schuler, B.; Qiu, D. Y.; Refaely-Abramson, S.; Kastl, C.; Chen, C. T.; Barja, S.; Koch, R. J.; Ogletree, D. F.; Aloni, S.; Schwartzberg, A. M.; Neaton, J. B.; Louie, S. G.; Weber-Bargioni, A. Large Spin-

- Orbit Splitting of Deep In-Gap Defect States of Engineered Sulfur Vacancies in Monolayer WS2. *Phys. Rev. Lett.* **2019**, *123*, 076801.
- (33) Cochrane, K. A.; Lee, J.-H.; Kastl, C.; Haber, J. B.; Zhang, T.; Kozhakhmetov, A.; Robinson, J. A.; Terrones, M.; Repp, J.; Neaton, J. B.; Weber-Bargioni, A.; Schuler, B. Spin-dependent vibronic response of a carbon radical ion in two-dimensional WS2. *Nat. Commun.* **2021**, 12, 7287
- (34) Liu, B.; Fathi, M.; Chen, L.; Abbas, A.; Ma, Y.; Zhou, C. Chemical Vapor Deposition Growth of Monolayer WSe2 with Tunable Device Characteristics and Growth Mechanism Study. *ACS Nano* **2015**, *9*, 6119–6127.
- (35) Zhang, X.; Choudhury, T. H.; Chubarov, M.; Xiang, Y.; Jariwala, B.; Zhang, F.; Alem, N.; Wang, G.-C.; Robinson, J. A.; Redwing, J. M. Diffusion-Controlled Epitaxy of Large Area Coalesced WSe2Monolayers on Sapphire. *Nano Lett.* **2018**, *18*, 1049–1056.
- (36) Mohn, F.; Schuler, B.; Gross, L.; Meyer, G. Different tips for high-resolution atomic force microscopy and scanning tunneling microscopy of single molecules. *Appl. Phys. Lett.* **2013**, *102*, 073109.
- (37) Hamann, D. R. Optimized norm-conserving Vanderbilt pseudopotentials. *Phys. Rev. B* **2013**, *88*, 085117.
- (38) Lebègue, S.; Arnaud, B.; Alouani, M.; Bloechl, P. E. Implementation of an all-electron GW approximation based on the projector augmented wave method without plasmon pole approximation: Application to Si, SiC, AlAs, InAs, NaH, and KH. *Phys. Rev. B* **2003**, *67*, 155208.
- (39) Kotani, T.; van Schilfgaarde, M. All-electron {GW} approximation with the mixed basis expansion based on the full-potential {LMTO} method. *Solid State Commun.* **2002**, *121*, 461–465
- (40) Del Ben, M.; da Jornada, F. H.; Antonius, G.; Rangel, T.; Louie, S. G.; Deslippe, J.; Canning, A. Static subspace approximation for the evaluation of G_0W_0 quasiparticle energies within a sum-over-bands approach. *Phys. Rev. B* **2019**, *99*, 125128.
- (41) da Jornada, F. H.; Qiu, D. Y.; Louie, S. G. Nonuniform sampling schemes of the Brillouin zone for many-electron perturbation-theory calculations in reduced dimensionality. *Phys. Rev. B* **2017**, *95*, 035109.